Photodissociation dynamics of OCS at 217 nm

Xilin Bai, Hao Liang, Zhengfang Zhou, Zefeng Hua, Dongfeng Zhao,* and Yang Chen[1]

Hefei National Laboratory for Physical Sciences at the Microscale, Department of Chemical Physics, and Synergetic Innovation Center of Quantum Information & Quantum Physics, University of Science and Technology of China, Hefei, Anhui 230026, PR China

ABSTRACT:

The $S(^1D_2)$ + $CO(X^1\Sigma^+)$ product channel from photodissociation of OCS at 217 nm has been measured using the DC slice velocity map imaging (VMI) technique in combination with resonance enhanced multiphoton ionization (REMPI). Two different REMPI intermediate states ($^1F_3$ and $^1P_1$) and several pump-probe laser polarization geometries are used to detect the angular momentum polarization of the phtofragmented $S(^1D_2)$. The molecular-frame polarization parameters, as well as the laboratory-frame anisotropy parameters, for individual rotational states of co-fragment CO, are determined using two different full quantum theories. The measured total kinetic energy release spectrum from photodissociation of OCS indicates two dissociation channels, corresponding to the fast and slow recoiling velocities of $S(^1D_2)$, respectively. The slow channel is concluded to originate from an initial photoexcitation to the $A(^1A')$ state, followed by a non-adiabatic transition to the ground state. The fast channel is found to follow a coherent excitation to $A(^1A')$ and $B(^1A'')$ states, where contributions of the two states are almost equal at 217 nm. The determined alignment and anisotropy parameters further indicate that the slow channel follows an incoherent excitation, while the fast channel follows a coherent excitation to $A(^1A')$ and $B(^1A'')$ states with a phase difference of $\pi/2$.

Keywords: Photodissociation dynamics, carbonyl sulfide, velocity map imaging

[1]Authors to whom correspondence should be addressed. Electronic mail: dzhao@ustc.edu.cn, yangchen@ustc.edu.cn.

1. INTRODUCTION:

The photodissociation of carbonyl sulfide (OCS) not only serves as a benchmark system for understanding the dissociation dynamics of triatomic molecules, but also plays a significant role in the stratosphere of earth's atmosphere.[1] OCS interacts strongly with ultraviolet radiation in the stratosphere, producing sulfur atoms that are involved in subsequent various atmospheric chemical evolution. Besides, OCS has also been identified in dense interstellar clouds and in comets.[2] As a consequence, many dedicated experimental[3-12] and theoretical[13-15] studies on the ultraviolet (UV) photochemistry have been performed over the past decades.

The first UV absorption band of OCS leads to two sulfur product channels, $S(^1D_2)$ and $S(^3P_j)$ channels, where the former dominates the dissociation process in the 193–248 nm region. The $S(^1D_2)$ channel is a spin-allowed dissociation pathway. It exhibits a bimodal translational energy distribution, which reflects two major components (fast channel and slow channel) of the accompanied photofragments CO. Because the C-O bond length (1.157 Å) in OCS is only a little longer than CO (1.128 Å), CO produced from OCS dissociation is liberated predominantly in its v = 0 state. In addition, the bending nature of the involved excited states after the photoexcitation yields highly rotational excitation in fragmented CO. With the increase of the excitation energy, the product rotational distribution moves to higher J, and the two components are merged together. Such experimental observations have been successfully modelled by McBane et al.[14] Based on the newly calculated potential energy surfaces (PESs), they also

predicted that the absorption cross sections for A(^{1}A′) and B(^{1}A″) states in the first absorption band region is roughly the same.

Suzuki et al.[16] investigated the anisotropy parameter β of this channel using a forward convolution analysis with inclusion of polarization effects of the photofragmented S(^{1}D$_2$). In that study, the velocity map imaging (VMI) technique was used to measure the velocity distributions of fragmented products, where the raw experimental images were processed using the commonly known inverse Abel transform method. However, this method may severely affect the accuracy of the derived polarization parameters, as the inverse Abel transform method is only suitable for reconstructions of experimental images with a cylindrical symmetry. Very recently, Weeraratna et al.[11] re-measured the anisotropic parameter β of the S(^{1}D$_2$) photoproduct via a (1+1)REMPI probe scheme with the [3s^{2}3p^3(^{4}S)4s]^{3}S intermediate state, which detection scheme is insensitive to the polarization effect. Limited by the REMPI detection scheme, atomic orbital polarization parameters of photofragmented S(^{1}D$_2$) cannot be determined from their experiment.

In a photodissociation reaction, the interaction between the parent molecule and a polarized light wave can result in polarization of the electronic angular momentum of atomic photofragments.[17-20] Detailed insight into the dynamics of the photodissociation process can be provided by a complete measurement of the polarization parameters of the atomic photofragments. Initially, Dixon et al.[21] introduced a semi-classical model

based on the bipolar harmonics approach, where a set of bipolar parameter are introduced to describe vector correlations in the photodissociation dynamics. E.g., the bipolar parameter $\beta_0^2(02)$ indicates the **μ**-**j** correlation which is a criteria to judge the symmetry of the excited state (e.g., A′ or A″) that leads to the measured photofragment. For an A′ state excitation, transition dipole moment **μ** lies in the OCS plane, **μ** and **j** must be perpendicular. In contrast, for an A″ state excitation, **μ** and **j** are both in the molecular plane. Therefore, the determination of the **μ**-**j** correlation can provide information about the relative contributions of the two absorption pathways. However, this theory cannot be used in the interpretation of photodissociation involving coherent photoexcitations.

A complete demonstration of the photodissociation dynamics has been developed with a full quantum treatment, initially introduced by Siebbeles et al.,[22] and later extended by Rakitzis and Zare.[23] In their treatment, the molecular-frame polarization parameters $a_q^{(k)}(p)$ (the label "p" refers to the symmetry of the type of the corresponding electronic transition) introduced by Rakitzis and Zare provide information of detailed photoexcitation and photodissociation mechanisms, both coherently and incoherently. E.g., $a_0^2(\parallel)$ and $a_0^2(\perp)$ describe contribution from incoherent parallel and perpendicular excitation, $a_2^2(\perp)$ describes contribution from coherent perpendicular excitation and $a_1^2(\parallel,\perp)$ describes the coherent excitation of a parallel and a perpendicular transition. This theory has been successfully applied to experimental studies on photodissociation dynamics of several molecules, such as

diatomic Cl_2, HCl, BrCl and O_2.[24, 25]

More recently, Suits and co-workers introduced a new set of laboratory-frame anisotropy parameters (see the review paper of Ref. 20), following a similar full quantum treat as made by Rakitzis and Zare. This set of laboratory-frame anisotropy parameters contains all information about the dissociation dynamics, and in principle, is an alternative form of the polarization parameters $a_q^{(k)}(p)$ introduced by Rakitzis and Zare. More importantly, this set of anisotropy parameters provide a new approach to process the VMI experimental data and to extract the important information about the dissociation dynamics.

Very recently, we have reported an experimental study in the photodissociation dynamics of OCS at 210 nm[26] using the DC slice velocity map imaging (VMI) technique in combination with resonance enhanced multiphoton ionization (REMPI). By comparing the experimental data obtained from dissociation wavelengths at 210 nm and 217 nm, a new dissociation channel involving excitation of the triplet c(^{3}A″) state is experimentally identified. In this paper, we present a complete experimental measurement on the kinetic energy distributions and angular distributions of S($^1D_2$) produced from photodissociation of OCS at 217 nm. Eight different polarization geometries of pump-probe laser and two REMPI detection schemes are used to obtain a complete characterization of the polarization effect of the photofragmented S($^1D_2$). The technique of high-resolution DC slice VMI makes it possible to determine the

molecular-frame polarization parameters and laboratory-frame anisotropy parameters following theories mentioned above. Based on the obtained anisotropy and polarization parameters, the photoexcitation and photodissociation mechanisms of OCS at 217 nm are also discussed.

2. EXPERIMENTAL DETAILS:

Experiments were performed using a home-built ion velocity map imaging setup, which has been described in detail previously.[27-29] Briefly, a molecular beam of OCS (5% OCS seeded in He), generated using a pulsed nozzle (General Valve, Series 9, 0.25 mm orifice) at a stagnation pressure of 1 bar, is skimmed and then expanded into a differentially pumped detection chamber. After passing through a hole which is 1 mm on the repeller plate, the molecular beam is directed along the TOF axis. Immediately following the photolysis, the photofragmented S($^1D_2$) atoms are ionized using a second UV laser beam via a (2+1)REMPI scheme. The photolysis and probe laser beams are aligned propagated to each other, and perpendicularly crossing the molecular beam between the repeller and extraction plates. Within a set of ion optics designed for the VMI measurements, the S^+ ions are accelerated by the focusing electric fields and projected onto a Chevron multichannel plate (MCP, Φ ~40 mm) detector coupled to a phosphor screen (P47). A fast high-voltage switch (PVM-4210, DEI; typical duration ~50 ns) is pulsed to gate the gain of the MCP's for mass selection as well as the time slicing of the ion packet. The transient images on the phosphor screen are captured by a charge-coupled device (CCD) camera (LaVision, Imager Intense, 1376 × 1024 pixels)

and then transferred to a computer on every shot for event counting and data analysis. Timing of the pulsed nozzle, the laser, and the pulsed gating is controlled by two multichannel digital delay pulse generators (DG 535, SRS).

For two-color laser experiments, OCS molecules are dissociated using a 217 nm linearly polarized laser, which is generated by the tripled output of a tunable dye laser (Sirah, PRSC-LG-18) that is pumped by a Nd:YAG laser (PRO-250, Spectra Physics, 532 nm) at a 10 Hz repetition rate. The polarization of the photolysis laser beam is adjusted by using a Berek's polarization compensator (New Focus, Model 5540), and checked by a MgF_2 Rochon prism. In order to avoid multiphoton processes, only about 0.3 mJ/pulse of the 217 nm laser is focused onto the OCS molecular beam by a f = 250 mm lens. The generated atomic fragments $S(^1D_2)$ are probed by an ionization laser produced by doubling the output of another tunable dye laser (Sirah, PrecisionScan), which is pumped from the third harmonic of a second Nd:YAG laser (GCR-170, Spectra Physics, 532 nm). An achromatic $\lambda/2$ or $\lambda/4$ waveplate (Thorlabs, 260–400 nm) is used to set the polarization of the probe laser at desired polarization. The probe laser is arranged to focus on the OCS photolysis region using a f = 200 mm lens. To avoid the Doppler effect of the recoiling velocity of photofragmented $S(^1D_2)$ atoms. Scanning of the probe laser wavelength in a small range, typically ~0.02 nm around each resonant wavelength, is performed during all image accumulations.

3. RESULTS AND DISCUSSION:

3.1. Results and analysis

Figs. 1 and 2 display the raw images of the S($^1D_2$) photoproducts recorded with the 217 nm photolysis of OCS. To obtain the full set of anisotropy and polarization parameters, two different REMPI transitions of S($^1D_2$) with eight different pump-probe laser polarization geometries are employed. These geometries are VV, VH, HV, HH, RR, RL, 45°R and 45°L, where the former letter represents the polarization of the pump laser, and the latter letter indicates the polarization of the probe laser. Here, the letter 'V' refers to a vertical direction of the laser polarization (i.e., the electrical field) that is in the plane of the slice image, 'H' a direction perpendicular to the detecting plane, '45°' indicates the laser linearly polarized in the middle of V and H, 'R' and 'L' the right and left circularly polarized light, respectively.

[INSERT FIGURE 1 HERE.]

[INSERT FIGURE 2 HERE.]

Each of the images represents a 2D projection of the recoiling velocity distribution of S($^1D_2$). The fine structure of the observed ring pattern is directly assigned to the internal energy distribution of the co-fragment CO. All the recorded images exhibit clear anisotropic structures, including a series of well resolved rings in the inner (slow channel) part, and one or two poorly resolved rings in the outer (fast channel) part. The total translational energy is calculated using the dissociation energy D_0 =34608 cm^{-1}[30] and using momentum and energy conservation laws in the two-body dissociation of a

unimolecular system. The rotational energy of CO(J) was calculated using the expression:

$$F(J)=B_vJ(J+1)-D_v J^2(J+1)^2 \quad (1)$$

in which accurate values for constants B_v and D_v are taken from Ref. 31. The rotational distribution obtained from our experiment show that the peak of slow channel locates at $J \approx 68$ and the fast channel locates at $J \approx 55$. It is noticed that, in Ref. 11, Weeraratna et al. found that the slow channel peaks at J = 71 and the fast channel at J = 59. The slightly different rotational population of photofragmented CO may be due to the different REMPI sensitivity factors for different REMPI detection schemes. As will be discussed below, in our experiment, the obtained rotational population of photofragmented CO exhibits a significant dependence on specific REMPI detection schemes of $S(^1D_2)$.

The total kinetic energy release (TKER, E_T) spectrum in the center-of-mass frame have been extracted by integrating the images over the whole angular range. Fig. 3 shows the obtained TKER spectra, all of which exhibit a bimodal structure that is similar with that of previously reported results at longer wavelengths. However, compared to that at longer dissociation wavelengths as presented in Refs. 3-10, the two components of the bimodal rotational distribution are almost merged together, and the rotational distribution moves to higher J. In addition, it is obviously seen that the relative intensity of the slow channel obtained with a vertically polarized photolysis laser is larger than that of horizontal polarization, i.e., the relative intensity of slow

channel depends strongly on the polarization direction of photolysis laser.

[INSET FIGURE 3 HERE.]

The atomic orbital polarization of S(^{1}D$_2$) from photodissociation shows up in Figs. 1 and 2. For experimental images recorded with one-photon dissociation and a (2+1) REMPI detection scheme, the measured angular distribution of the S(^{1}D$_2$) atoms, $I(\theta)$, can be extracted by integrating a three-dimensional velocity distribution over an appropriate range of speed at each angle. The angular distribution is then fitted using the formula:

$$I(\theta) = 1 + \beta_2 P_2(cos\theta) + \beta_4 P_4(cos\theta) + \beta_6 P_6(cos\theta), \quad (2)$$

where β_2, β_4 and β_6 are the expansion coefficients, $P_2(cos\theta)$, $P_4(cos\theta)$ and $P_6(cos\theta)$ are the second, fourth and sixth order Legendre polynomial expansions, respectively. The obtained Legendre polynomial coefficients $\beta_{2,4,6}$ for individual rings are summarized in Table 1. Because only one parameter is found to be necessary to describe the angular distributions of S(^{1}D$_2$) products under VH pump-probe laser polarization geometry, only β_2 parameters for VH geometry are listed in Table 1. Here, we label the fully resolved rings using the rotational quantum numbers of the co-fragment CO(J). For the poorly resolved parts (fast channel), i.e., CO (J = 48 – 60) as indicated in Fig. 3, J values are grouped with several adjacent J values in the analysis.

[INSERT TABLE 1 HERE.]

Using the full set of the $\beta_{2,4,6}$ values in Table 1 and following the theoretical model described by Rakitzis and Zare, the β parameter and the molecular-frame polarization parameters $a_q^{(k)}(p)$ of S(^{1}D$_2$) from 217 nm photodissociation of OCS have been determined, and the results are listed in Table 2. We have also processed the raw experimental images as described in Ref. 6, from which the full set of laboratory-frame anisotropy parameters are determined. Table 3 summarizes the obtained anisotropy parameters. Using the relations between the molecular-frame polarization parameters and the laboratory-frame anisotropy parameters as discussed in Ref. [20], we find that the two sets of parameters listed in Tables 2 and 3 are well consistent with each other. The consistency indicates that the parameters determined here are reliable, and can be used to interpret the detailed photoexcitation and photodissociation mechanisms of OCS at 217 nm.

[INSERT TABLE 2 HERE.]

[INSERT TABLE 3 HERE.]

3.2. Photoexcitation and photodissociation mechanisms

The tendency of the observed bimodal rotational distribution is consistent with the complete trajectory surface hopping calculation by Wei et al.[12] that the bimodal rotational distribution merged together and higher rotational will be distributed with increasing excitation energy. The higher rotational excitation of co-fragment CO indicates that the excited parent molecule has a larger torque at this wavelength, which

has been proven by Schmidt et al.[14] using the reconstructed potential energy surfaces. The anisotropy parameter β we obtained are slightly lower than that reported in Ref. 11. As discussed by Suzuki et al., this indicates that the alignment effects must be considered for a precise analysis.[16]

The anisotropy parameter β for the slow channel is found to be ~1.5 (close to +2), indicating that the photoexcitation is dominated by a parallel transition to the A(^{1}A′) state. This is further supported by two addition arguments. Firstly, for this channel, **μ**-**j** correlation parameter $\beta_0^2(02)$ is negative, i.e., the transition dipole momentum **μ** is perpendicular to the orbital angular momentum **j** of the photofragmented S(^{1}D$_2$), which is well consistent with a parallel photoexcitation.[32] Secondly, the relative intensity of the slow channel component shows a clear dependence on the polarization of the photolysis laser. Specifically, a vertical polarization results in a larger intensity than a horizontal polarization, where the latter is commonly known to be inefficient for detecting a parallel transition by VMI. Based on these experimental results and previous theoretical predictions,[14] we conclude that the slow channel originates from an initial photoexcitation to the A(^{1}A′) state, followed by a non-adiabatic transition to the ground state.

Compared to the slow channel, the anisotropy parameter β of the fast channel are significantly smaller, indicating that the fast channel arises from a mixed electronic transitions. Using the minimum value of β ~0.36 at CO (J ≈ 53, almost the center of

the fast component), we estimate that the contributions of the perpendicular and parallel transition components are comparable for the fast channel. Further evidences from our experiment are also available in support of this conclusion. First of all, the **μ-j** correlation parameters for the fast channel $\beta_0^2(02)$ are close to 0.25, indicating mixed excitation of the A(^{1}A′) and B(^{1}A″) states. This is also consistent with the interpreted bimodal distribution based on the anisotropy parameter β. Secondly, the relative intensity of the fast channel has nearly no change under both the horizontal and vertical polarized photolysis laser, illustrating that this channel arises from a mixed perpendicular-parallel transition, and contributions of the two transitions are comparable. In addition, the interpretation is also well consistent with the trajectory surface-hopping calculations recently reported by McBane et al.[14] Therefore, the observed fast channel results from a simultaneous excitation of repulsive A(^{1}A′) and B(^{1}A″) states followed by a rapid dissociation process.

Based on the theoretical models as demonstrated in Ref. 33, the obtained polarization and anisotropy parameters allow us to determine the phase differences between different dissociation channels. Here, the obtained molecular-frame polarization parameters a_1^2 and a_2^2 and laboratory-frame anisotropy parameters η_2 and γ_2, all of which are correlated to the real part of the coherent excitation term, are constrained to zero. The nearly zero values of these parameters suggest that the photodissociation dynamics follows an incoherent excitation (i.e., no coherent terms) or a coherent excitation with a phase difference of π/2 (i.e., the real part of the coherent term is 0).

In addition, our experimental images recorded under RR, RL, 45°R and 45°L pump-probe laser polarization geometries have allow us to determine the values of γ_1' that is correlated to the imaginary part of the coherent term. We find that, values of the parameter γ_1' for the slow channel are also constrained to 0, but not for the fast channel. Therefore, we conclude that the slow channel follows an incoherent excitation to the A(^{1}A′) state, while the fast dissociation channel follows a coherent excitation to A(^{1}A′) and B(^{1}A″) states with a phase difference of π/2.

4. CONCLUSIONS

Based on a complete experimental measurement of S($^1D_2$) from photodissociation of OCS at 217 nm by VMI, we have determined both molecular-frame polarization parameters and laboratory-frame anisotropy parameters. The measured total kinetic energy release spectrum from photodissociation of OCS indicate two dissociation channels of the fragmented S($^1D_2$), the fast and slow recoiling velocities of S($^1D_2$), respectively.. The slow channel is concluded to originate from an initial photoexcitation to the A(^{1}A′) state, followed by a non-adiabatic transition to the ground state. The fast channel is found to follow a coherent excitation to A(^{1}A′) and B(^{1}A″) states, where contributions of the two states are almost equal. The determined alignment and anisotropy parameters further indicate that the slow channel follows an incoherent excitation, while the fast channel follows a coherent excitation to A(^{1}A′) and B(^{1}A″) states with a phase difference of π/2.

ACKNOWLEDGMENTS

This work is financially supported by MOST-NBRPC (2010CB923302 and 2013CB834602), NSFC (21273212, 21173205, and 91127042), and the Fundamental Research Funds for the Central Universities.

References

[1] J. Notholt, Z. Kuang, C. P. Rinsland, G. C. Toon, M. Rex, N. Jones, T. Albrecht, H. Deckelmann, J. Krieg, C. Weinzierl, H. Bingemer, R. Weller, and O. Schrems, Science **300**, 307 (2003).

[2] P. Ehrenfreund, and S. B. Charnley, Annu. Rev. Astron. Astrophys. **38**, 427 (2000).

[3] G. Nan, I. Burak, and P. L. Houston, Chem. Phys. Lett. **209**, 383 (1993).

[4] Y. Sato, Y. Matsumi, M. Kawasaki, K. Tsukiyama, and R. Bersohn, J. Phys. Chem. **99**, 16307 (1995).

[5] Z. H. Kim, A. J. Alexander, and R. N. Zare, J. Phys. Chem. A **103**, 10144 (1999).

[6] T. P. Rakitzis, P. C. Samartzis, and T. N. Kitsopoulos, Phys. Rev. Lett. **87**, 123001 (2001).

[7] A. J. van den Brom, T. P. Rakitzis, and M. H. M. Janssen, J. Chem. Phys. **121**, 11645 (2004).

[8] S. K. Lee, R. Silva, S. Thamanna, O. S. Vasyutinskii, and A. G. Suits, J. Chem. Phys. **125**, 144318 (2006).

[9] M. Brouard, F. Quadrini, and C. Vallance, J. Chem. Phys. **127**, 084305 (2007).

[10] M. L. Lipciuc, T. P. Rakitzis, W. L. Meerts, G. C. Groenenboom, and M. H. Janssen, Phys. Chem. Chem. Phys. **13**, 8549 (2011).

[11] C. Weeraratna, C. Amarasinghe, R. Fernando, V. Tiwari, and A. G. Suits, Chem. Phys. Lett. **657**, 162 (2016).

[12] W. Wei, C. J. Wallace, G. C. McBane, and S. W. North, J. Chem. Phys. **145**, 024310 (2016).

[13] J. A. Schmidt, M. S. Johnson, G. C. McBane, and R. Schinke, J. Chem. Phys. **136**, 131101 (2012).

[14] G. C. McBane, J. A. Schmidt, M. S. Johnson, and R. Schinke, J. Chem. Phys. **138**, 094314 (2013).

[15] J. A. Schmidt, and J. M. Olsen, J. Chem. Phys. **141**, 184310 (2014).

[16] T. Suzuki, H. Katayanagi, S. Nanbu, and M. Aoyagi, J. Chem. Phys. **109**, 5778 (1998).

[17] A. J. Orrewing, and R. N. Zare, Annu. Rev. Phys. Chem. **45**, 315 (1994).

[18] T. P. Rakitzis, P. C. Samartzis, R. L. Toomes, T. N. Kitsopoulos, A. Brown, G. G. Balint-Kurti, O. S. Vasyutinskii, and J. A. Beswick, Science **300**, 1936 (2003).

[19] T. P. Rakitzis, A. J. van den Brom, and M. H. M. Janssen, Science **303**, 1852 (2004).

[20] A. G. Suits, and O. S. Vasyutinskii, Chem. Rev. **108**, 3706 (2008).

[21] R. N. Dixon, J. Chem. Phys. **85**, 1866 (1986).

[22] L. D. A. Siebbeles, M. Glassmaujean, O. S. Vasyutinskii, J. A. Beswick, and O. Roncero, J. Chem. Phys. **100**, 3610 (1994).

[23] T. P. Rakitzis, and R. N. Zare, J. Chem. Phys. **110**, 3341 (1999).

[24] T. Peter Rakitzis, S. Alex Kandel, Andrew J. Alexander, Zee Hwan Kim, and Richard N. Zare, J. Chem. Phys. **110**, 3351 (1999).

[25] A. J. Gilchrist and G. A. D. Ritchie, J. Chem. Phys. **138**, 214307 (2013).

[26] Xilin Bai, Hao Liang, Zhengfang Zhou, Zefeng Hua, Bin Jiang, Dongfeng Zhao, and Yang Chen, J. Chem. Phys. **147**, 013930 (2017).

[27] R. Mao, Q. Zhang, J. Zang, Z. Zhang, C. He, C. Qin, Y. Chen, Chin. J. Chem. Phys. **24**, 631 (2011).

[28] R. Mao, Q. Zhang, J. Zang, C. He, M. Chen, and Y. Chen, J. Chem. Phys. **135**, 244302 (2011).

[29] Z. Gu, M. Chen, C. He, X. Bai, R. Mao, Q. Zhang, Y. Chen, Chin. J. Chem. Phys. **26**, 493 (2013).

[30] M. Laura Lipciuc and Maurice H. M. Janssen, Phys. Chem. Chem. Phys. **8**, 3007 (2006).

[31] P. Cacciani, F. Brandi, I. Velchev, C. Lynga, C. G. Wahlstrom, and W. Ubachs, Eur. Phys. J. D. **15**, 47 (2001).

[32] M. P. Grubb, M. L. Warter, C. D. Freeman, N. A. West, K. M. Usakoski, K. M. Johnson, J. A. Bartz, and S. W. North, J. Chem. Phys. **135**, 094201 (2011).

[33] T. P. Rakitzis, and A. J. Alexander, J. Chem. Phys. **132**, 224310 (2010).

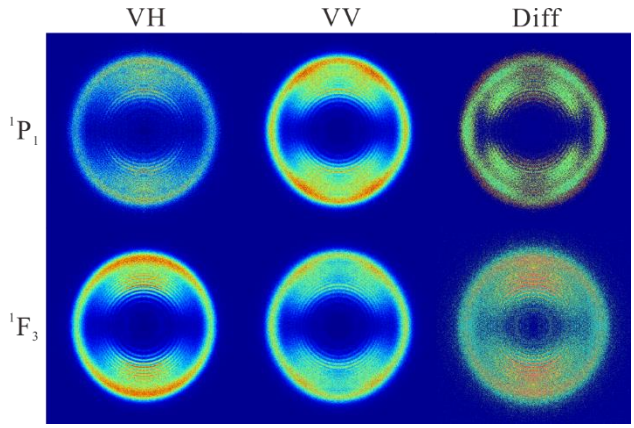

Fig. 1 Raw images of S($^1D_2$) in the photodissociation of OCS at 217 nm. Red and green correspond to positive and negative signal intensities for difference images, respectively.

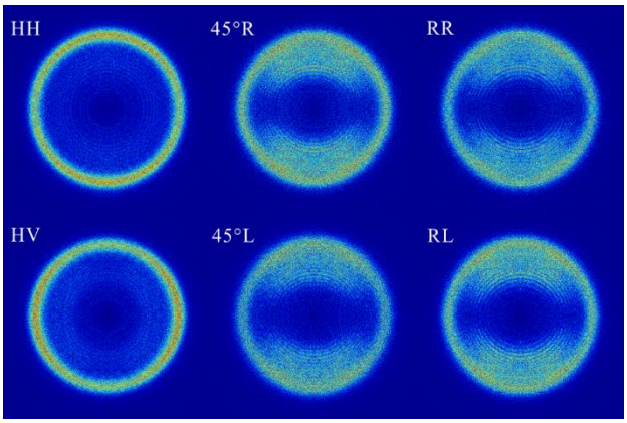

Fig. 2 Raw images of S($^1D_2$) in the photodissociation of OCS at 217 nm through $^1F_3$ resonant intermediate state.

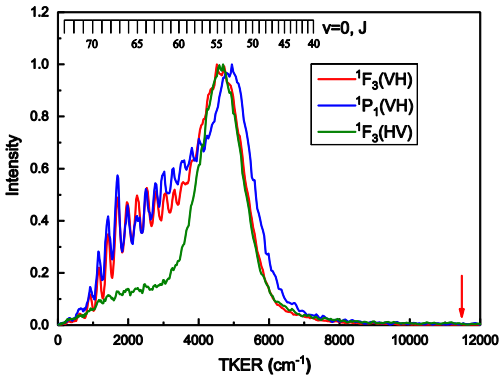

Fig. 3 Total kinetic energy distributions in the photodissociation of OCS at 217 nm. The vertical red arrow indicates the available energy (the photolysis photon energy less that required for C–S bond fission) of S($^1D_2$) channel at 217 nm photodissociation.

Table 1 The determined Legendre polynomial coefficients, β_2, β_4 and β_6, from the angular distribution of photofragmented $S(^1D_2)$ at 217 nm.

	VV($^1F_3$)			**VH($^1F_3$)**	**VV($^1P_1$)**			**VH($^1P_1$)**
J_{CO}[a]	β_2	β_4	β_6	β_2	β_2	β_4	β_6	β_2
71	0.78	-0.04	-0.06	0.85	0.83	-0.13	0.05	0.74
70	0.97	-0.08	-0.09	1.19	1.08	-0.18	-0.03	1.1
69	1.11	-0.18	-0.01	1.35	1.22	-0.16	0	1.32
68	1.19	-0.21	0.03	1.55	1.33	-0.2	0.04	1.43
67	1.23	-0.18	0.04	1.67	1.35	-0.26	0.05	1.5
66	1.22	-0.26	-0.05	1.59	1.18	-0.56	-0.14	1.38
65	1.2	-0.26	-0.03	1.59	1.18	-0.58	-0.15	1.36
64	1.18	-0.19	-0.06	1.55	1.22	-0.53	-0.18	1.35
63	1.17	-0.21	-0.02	1.51	1.25	-0.48	-0.17	1.33
62	1.18	-0.22	-0.03	1.47	1.29	-0.37	-0.2	1.34
61	1.03	-0.21	-0.03	1.37	1.2	-0.29	-0.15	1.26
58*[b]	0.63	-0.14	-0.05	0.91	0.78	-0.19	-0.2	0.89
56*[b]	0.29	-0.1	-0.04	0.49	0.35	-0.13	-0.25	0.39
53*[b]	0.24	-0.02	-0.07	0.38	0.23	0.06	-0.24	0.36
48*[b]	0.63	0.15	-0.03	0.79	0.72	0.37	-0.09	0.82

[a]The corresponding rings in the raw images are labelled using the correlated rotational quantum number J of co-fragment CO(J).

[b]Asterisks (*) indicates the J values are grouped with several adjacent J values for the poorly resolved part in the raw image.

Table 2 The molecular-frame polarization parameters $a_q^{(k)}(p)$ and the derived bipolar momentum parameters $\beta_0^2(02)$ of photofragmented S($^1D_2$) at 217 nm.

J_{CO}[a]	β	$a_0^2(\parallel)$	$a_0^2(\perp)$	a_1^2	$a_2^2(\perp)$	$a_0^4(\parallel)$	$a_0^4(\perp)$	a_1^4	$a_2^4(\perp)$	$\beta_0^2(02)$
71	0.83	-0.05	0.01	0	0	0.01	0.01	0.02	-0.02	-0.02
70	1.14	-0.13	-0.18	0	0	0.03	0.07	0.02	0.04	-0.03
69	1.17	-0.15	0.50	0	0	0.02	0.30	-0.02	0.09	-0.09
68	1.37	-0.20	0.39	0	0	0.03	0.34	0.02	0.13	-0.10
67	1.53	-0.21	-0.22	0	0	0.04	0.30	0.06	0.18	-0.08
66	1.40	-0.20	0.58	0	0	0.07	0.47	0.02	0.19	-0.11
65	1.40	-0.21	0.44	0	0	0.08	0.45	0.03	0.18	-0.11
64	1.43	-0.19	-0.06	0	0	0.07	0.33	0.03	0.16	-0.08
63	1.35	-0.19	0.29	0	0	0.06	0.36	0.00	0.14	-0.09
62	1.29	-0.18	0.49	0	0	0.05	0.36	-0.03	0.13	-0.10
61	1.19	-0.21	0.30	0	0	0.05	0.30	-0.02	0.12	-0.10
58*[b]	0.78	-0.20	0.06	0	0	0.05	0.16	-0.02	0.08	-0.07
56*[b]	0.41	-0.19	0.04	0	0	0.06	0.06	-0.02	0.04	-0.05
53*[b]	0.36	-0.11	-0.09	0	0	0.05	0.00	-0.01	0.04	-0.01
48*[b]	0.91	-0.06	-0.88	0	0	0.00	-0.23	0.06	0.02	0.06

[a]The corresponding rings in the raw images are labelled using the correlated rotational quantum number J of co-fragment CO(J).

[b]Asterisks (*) indicates the J values are grouped with several adjacent J values for the poorly resolved part in the raw image.

Table 3 The anisotropy parameters of photofragmented S($^1D_2$) at 217 nm.

J_{CO}[a]	β	α_2	S_2	γ_2	η_2	α_4	S_4	γ_4	η_4
71	0.83	0.01	-0.01	0	0	0.00	0.00	-0.01	0.01
70	1.14	0.01	-0.03	0	0	0.00	0.00	-0.02	-0.01
69	1.17	0.04	0.01	0	0	-0.01	0.02	0.01	-0.03
68	1.37	0.04	-0.02	0	0	0.00	0.02	-0.01	-0.03
67	1.53	0.03	-0.04	0	0	0.00	0.00	-0.04	-0.03
66	1.40	0.04	-0.01	0	0	0.00	0.01	-0.01	-0.04
65	1.40	0.04	-0.02	0	0	0.01	0.01	-0.02	-0.04
64	1.43	0.03	-0.03	0	0	0.01	0.00	-0.02	-0.03
63	1.35	0.04	-0.02	0	0	0.00	0.01	0.00	-0.03
62	1.29	0.04	0.00	0	0	0.00	0.02	0.02	-0.03
61	1.19	0.04	-0.01	0	0	0.00	0.02	0.01	-0.04
58[*b]	0.78	0.03	-0.02	0	0	0.00	0.01	0.02	-0.04
56[*b]	0.41	0.02	-0.01	0	0	0.01	0.00	0.02	-0.03
53[*b]	0.36	0.01	-0.02	0	0	0.01	-0.01	0.01	-0.03
48[*b]	0.91	-0.03	-0.07	0	0	0.01	-0.03	-0.04	-0.01

[a]The corresponding rings in the raw images are labelled using the correlated rotational quantum number J of co-fragment CO(J).

[b]Asterisks (*) indicates the J values are grouped with several adjacent J values for the poorly resolved part in the raw image.